ELSEVIER

PII: S0032-3861(97)00487-4

Polymer Vol. 39 No. 10, pp. 2023–2033, 1998

0032-3861/98/$19.00+0.00

Microstructure of block copolymers of polystyrene and poly(ethylene-*alt*-propylene)

Sudhir Mani†[a], R. A. Weiss[a,*], S. F. Hahn[b], C. E. Williams[c], M. E. Cantino[d] and L. H. Khairallah[d]

[a]*Department of Chemical Engineering and Polymer Science Program, University of Connecticut, Storrs, CT 06269, USA*
[b]*Central Research—Advanced Polymeric Systems Laboratory, The Dow Chemical Company, Midland, MI 48674, USA*
[c]*Laboratoire des Fluides Organises, CNRS URA 792, College de France, 11 Place Marcelin-Berthelot, 75231 Paris Cedex 05, France*
[d]*Electron Microscopy Laboratory, Department of Physiology and Neurobiology, University of Connecticut, Storrs, CT 06269, USA*
(Received 10 January 1997; revised 29 May 1997)

The microstructure and microphase behaviour of diblock ($M_n \approx 27$ and 50 kg mol^{-1}) and triblock ($M_n \approx 50$ kg mol^{-1}) copolymers of polystyrene (PS) and poly(ethylene-*alt*-propylene) (PEP) were studied by small-angle X-ray scattering (SAXS), transmission electron microscopy (TEM) and dynamic mechanical thermal analysis (DMTA). The composition was varied from 10 wt.% to 50 wt.% PS. The morphology of solution-cast and compression-moulded samples was compared. The common packing arrangements of body-centred-cubic (BCC) spheres, hexagonal-close-packed (HCP) cylinders and alternating lamellae were observed for the PS microdomains using SAXS and TEM. A microphase texture of PS spheres with a liquid-like packing (LLP) was obtained at lower molecular weight and PS content. Coexisting textures of LLP spheres and HCP cylinders of PS were observed in a triblock copolymer with low PS content. An order–order transition between conventional lamellar and perforated lamellar textures was detected in a nearly-symmetric triblock copolymer. Conventional order–disorder transitions were identified for most of the other polymers using DMTA and temperature-resolved SAXS.

(Keywords: block copolymer; microstructure)

INTRODUCTION

Microphase separation occurs in block copolymers because of the thermodynamic immiscibility between the chemically dissimilar homopolymer blocks that are covalently connected. Highly regular, self-assembled textures such as body-centred-cubic-packed (BCC) spheres, hexagonal-close-packed (HCP) cylinders, ordered bicontinuous phases and alternating lamellar phases have been theoretically predicted and experimentally observed[1–10]. Other microphase textures have also been observed, including lamellar-catenoid[11], also referred to as 'mesh'[12] or perforated layer[13–17] phases, and a modulated lamellar or 'rippled lamellar' phase[13–15]. The specific texture achieved with a particular system depends on the copolymer composition, molecular weight, copolymer architecture, intensity of the repulsive interactions between the chemically dissimilar blocks as characterized by the Flory χ-parameter, and the method of sample preparation.

At elevated temperatures, block copolymers may exhibit an order-to-disorder transition (ODT) where the self-assembled microphase disorders into a spatially homogeneous state[1]. The ODT is also referred to as the microphase separation transition (MST), which identifies the onset of formation of an ordered microphase as the disordered melt is cooled. Theoretically, the ODT and MST should occur at the same temperature, though they may not correspond experimentally due to kinetic effects. Other transitions in which the ordered microphase texture of a block copolymer changes, termed mesophase transitions or order-to-order transitions (OOTs), may also occur[13–19].

In this paper, we describe the microstructure and microphase behaviour of diblock and triblock copolymers of polystyrene (PS) and poly(ethylene-*alt*-propylene) (PEP). The copolymer composition was varied between *ca.* 10–50 wt.% PS and polymers with two different molecular weights, *ca.* 27 kg mol^{-1} and *ca.* 50 kg mol^{-1}, were studied. Synchrotron small-angle X-ray scattering (SAXS) and transmission electron microscopy (TEM) were used to identify the room-temperature microphase texture, and temperature-resolved SAXS was employed to study the microstructural evolution of the block microphase with increasing temperature and to identify microphase transitions. Dynamic mechanical thermal analysis (DMTA) was also used to characterize the microphase transitions. The effect of sample preparation on the microstructural development of the block copolymers was determined by comparing solution-cast and compression-moulded samples.

* To whom correspondence should be addressed
† Present address: Department of Chemical Engineering, Imperial College of Science, Technology and Medicine, Prince Consort Road, London SW7 2BY, UK

EXPERIMENTAL DETAILS

Polymer synthesis and sample preparation

PS/PEP block copolymers were prepared by anionic polymerization of block copolymers of PS and polyisoprene (PI) followed by selective hydrogenation of the PI blocks. Because the isoprene polymerized primarily from 1,4-additions, the hydrogenated polymer was essentially an alternating copolymer of ethylene and propylene. The block copolymers studied are summarized in *Table 1*. The samples denoted SEP*x*, 27SEP*x* and SEPS*x* correspond to diblock copolymers with $M_n = 50$ kg mol^{-1}, diblock copolymers with $M_n = 27$ kg mol^{-1} and triblock copolymers with $M_n = 50$ kg mol^{-1}, respectively, where S stands for PS, EP for PEP and *x* denotes the copolymer composition in wt.% PS.

Anionic polymerization of PS–PI diblock copolymers was performed in a 1500 ml glass polymerization reactor that was cleaned with refluxing cyclohexane and evacuated at 85°C under vacuum prior to use. In an example polymerization, 700 ml of cyclohexane was passed through activated alumina into the reactor. The solvent was titrated to a persistent colour with a difunctional initiator prepared from 1,3-bis(1-phenyl ethenyl) benzene and sec-butyl lithium[20–25]. To this was added 80 g isoprene monomer, distilled away from dibutyl magnesium prior to use. The reactor temperature was raised to 50°C and the polymerization was initiated by the addition of 7.3 ml of a 0.55 M sec-butyl lithium solution in cyclohexane. The polymerization was allowed to proceed for 45 min, after which an analytical sample was taken and quenched in methanol. 20 g styrene, distilled away from CaH_2 prior to use, was added to the reactor, and styrene polymerization was allowed to proceed for 30 min and then terminated with 1 ml isopropanol. Under these polymerization conditions, the block copolymer contained about 8–10% of 3,4-isoprene units, as determined by ^{1}H-NMR analysis.

The procedure for the synthesis of PS–PI–PS triblock copolymers was similar, except that a difunctional initiator was used. As an example, 700 ml of cyclohexane and 0.7 ml of a 0.5 M solution of pentamethyl diethylene triamine (PMDETA) were added to the reactor and titrated to a persistent colour with the same difunctional initiator used in the diblock synthesis. 90 g isoprene was then added to the reactor and the temperature was raised to 55°C. Polymerization was initiated by the addition of 30 g of a 0.0759 mmole g^{-1} difunctional initiator solution in cyclohexane. At the completion of the isoprene polymerization, 10 g styrene was added to the reactor. Styrene polymerization was allowed to proceed for 45 min and then terminated with 1 ml isopropanol.

The diene block was hydrogenated in a 1000 ml pressure reactor that was cleaned and dried prior to use. In a typical hydrogenation reaction, 50 g of PS–PI diblock copolymer in 400 ml of a cyclohexane was added to the pressure reactor. The solution was diluted with 100 ml cyclohexane passed over activated alumina, and the solution was deoxygenated with repetitive evacuation/nitrogen refill cycles. The reaction vessel was then pressurized to 300 psig with H_2 gas. A catalyst solution was prepared in a 100 ml round bottom single neck flask equipped with a magnetic stirrer and septum port[26–28]. The flask was evacuated and refilled with dry nitrogen, and 20 ml of a 0.1 M nickel 2-ethyl hexanoate solution in cyclohexane, obtained from Shepard Chemical as a 10% nickel solution in mineral spirits and diluted to the desired concentration, was added. The solution was stirred and 2.4 ml of a 1.9 M triethyl aluminum solution in heptane was added dropwise, forming a black suspension. This suspension was transferred by syringe to the reactor, which was heated to 65°C and pressurized to 300 psig with H_2. The reaction was allowed to proceed for 24 h; the reactor was repressurized with H_2 to 300 psig when it dropped below 250 psig. After 24 h, the excess H_2 was vented and the polymer solution was drained from the reactor. The polymer solution was stirred in contact with a 10% aqueous citric acid solution until the catalyst colour disappeared (about 24 h), after which the polymer solution was separated and filtered through a sintered glass funnel. The polymer was isolated by precipitation into methanol and was dried in a vacuum oven for 4 h at 100°C to remove residual solvents. ^{1}H-NMR analysis showed no detectable residual olefin. For the copolymers containing *ca.* 50 wt.% PS, complete saturation required additional catalyst loading and longer reaction times.

Nuclear magnetic resonance (NMR) analyses were performed with 5% (w/v) polymer solutions in $CDCl_3$ using a 300 MHz Varian Gemini 300 NMR spectrometer. Gel permeation chromatography (GPC) was performed with tetrahydrofuran using a flow rate of 1 ml min^{-1} through six columns, three single-pore and three mixed-bed, and u.v. and differential refractometer detectors. The g.p.c. was calibrated using narrow-molecular-weight polystyrene and polyisoprene samples.

Films were prepared either by solution casting or compression moulding. Solution-cast samples were

Table 1 Molecular characteristics of the block copolymers

Designation	Architecture	w_{PS} [a]	ϕ_{PS} [b]	M_n (Dalton)s [c]	M_w/M_n [c]
SEP10	Diblock	0.108	0.089	48 200	1.03
SEP20	Diblock	0.203	0.171	54 000	1.04
SEP35	Diblock	0.356	0.309	52 000	1.03
SEP50	Diblock	0.504	0.452	52 000	1.04
SEPS9	Triblock	0.090	0.074	54 900	1.16
SEPS21	Triblock	0.215	0.182	49 300	1.08
SEPS50	Triblock	0.508	0.456	50 000	1.12
27SEP10	Diblock	0.097	0.080	27 680	1.02
27SEP18	Diblock	0.184	0.155	26 900	1.02
27SEP50	Diblock	0.498	0.446	26 620	1.02

[a] Weight fraction of PS phase, determined by ^{1}H NMR.
[b] Volume fraction of PS phase, calculated using $\phi_{PS} = \{1 + (d_{PS}/d_{PEP})[(1/w_{PS}) - 1]\}^{-1}$, where d_i is the mass density of phase "i", i = PS or PEP. Values of $d_{PS} = 1.06$ and $d_{PEP} = 0.86$ g cm^{-3} were used[46].
[c] Determined by g.p.c.

prepared by evaporating the solvent from 10% (w/v) solutions of the block copolymer in toluene in partially covered glass dishes over a period of 7 days. Since toluene is a good solvent for both homopolymer blocks, it was expected that the samples prepared in this way would possess a microstructure close to equilibrium. The cast films were peeled off the glass and dried to constant weight at 50°C under vacuum. A Carver laboratory press was used to compression-mould samples at 200°C and *ca.* 4.4 MPa pressure. The moulded films were cooled to room temperature between the platens of the press at a rate of $\sim 1°C\ min^{-1}$ while maintaining a constant pressure. The compression-moulded samples were dried to constant weight at 50°C under vacuum. All the film specimens were annealed at 100°C for 24 h, except for SEPS9, 27SEP10 and 27SEP18, which were annealed at 70°C for 24 h.

Small-angle X-ray scattering

Beamline D22 at the DCI-LURE synchrotron radiation source in Orsay, France was used for SAXS measurements. A description of the beamline optics is available elsewhere[29]. The detector was a gas-filled position-sensitive proportional counter. A modified Mettler FP5 microscopy hot-stage with a temperature range of 40–280°C was used for temperature-resolved measurements. Two different experimental conditions were used: (1) an X-ray wavelength, λ, of 0.1377 nm and a sample-to-detector distance (SDD) of 1.252 m or 1.522 m, and (2) λ = 0.1458 nm and SDD = 1.560 m for room-temperature experiments or SDD = 1.608 m for temperature-resolved measurements. The SAXS data were corrected for parasitic scattering, incident beam decay, sample absorption and thermal background, and are presented in relative units. Conversion to absolute intensity requires a simple multiplicative factor. The beamline optics were such that desmearing corrections were not required.

Dynamic mechanical thermal analysis

Dynamic storage and loss moduli, G' and G'', were measured with a Polymer Laboratories' PL-DMTA Mk II using a shear-sandwich test fixture (7 mm diameter shear studs), heating rates between $0.2–1.0°C\ min^{-1}$, strains of 0.5–1.3% and a frequency of 0.1 Hz. A nitrogen atmosphere was used to minimize oxidative degradation of the sample. GPC analysis of specimens that were heated above 200°C during DMTA or SAXS experiments indicated that little degradation of the block copolymers occurred.

Transmission electron microscopy

TEM micrographs were obtained with a Philips EM300 transmission electron microscope using an accelerating voltage of 80 kV. Two different specimen preparations were used. For some samples, small slivers of copolymer were stained by immersion for 48 h in a 0.5% aqueous ruthenium tetroxide (RuO_4) solution in a sealed vial. Fresh solution was added after 24 h. RuO_4 preferentially stains the PS, which also hardens the polymer and enhances the electron contrast between the two microphases. The stained polymer was embedded in a mixture of Araldite 502 and Epon 812 epoxy resins, and thin sections were microtomed at room temperature using a LKB Ultratome V microtome equipped

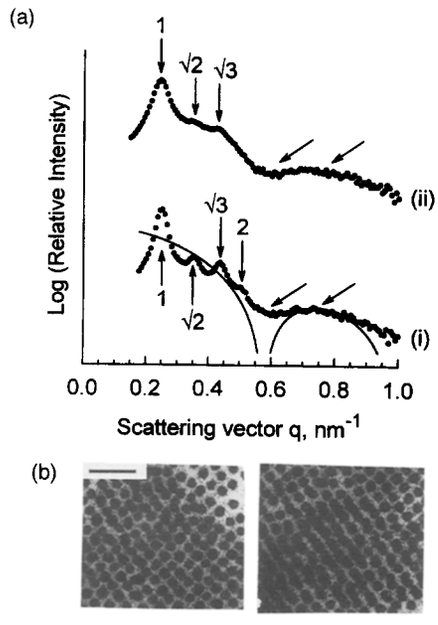

Figure 1 Microphase texture of SEP10 diblock copolymer. (a) Room temperature SAXS curve for (i) solution-cast and (ii) compression-moulded samples. In these and all subsequent SAXS curves, vertical arrows indicate maxima of the structure factor, $S(q)$, with the corresponding values of q_m/q^* as shown, and diagonal arrows indicate minima and maxima of the particle form factor, $P(q)$. The solid line represents the theoretical $P(q)$ function for a hard sphere of radius R = 7.8 nm. (b) TEM micrographs showing orthogonal views of the spherical PS domains in (i) solution-cast and (ii) compression-moulded SEP10. The scale bar of 100 nm applies to both micrographs. The dark and light regions in these and the other micrographs in this paper correspond to the PS phase stained by RuO_4 and the unstained PEP phase, respectively

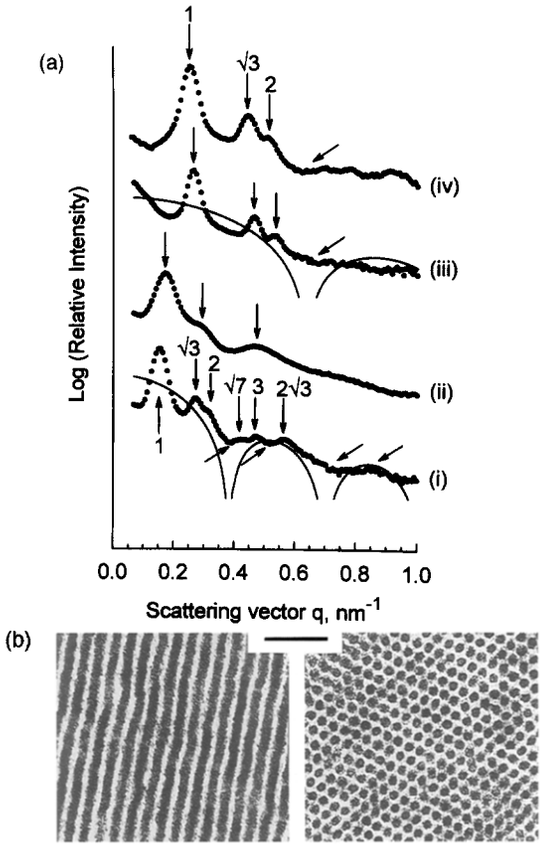

Figure 2 Microphase texture of PS cylinders. (a) Room-temperature SAXS curve for (i) SEP20 (SC), (ii) SEP20 (CM), (iii) SEPS21 (SC), (iv) SEPS21 (CM). SC and CM refer to solution-cast and compression-moulded samples, respectively, in this and all subsequent figures. The solid line represents the theoretical $P(q)$ function for an infinitely long cylinder of radius R = 10.0 nm (curve (i)) and R = 6.0 nm (curve (iii)). (b) TEM micrographs showing orthogonal views of the texture of PS cylinders for the SEPS21(SC). The scale bar corresponds to 100 nm

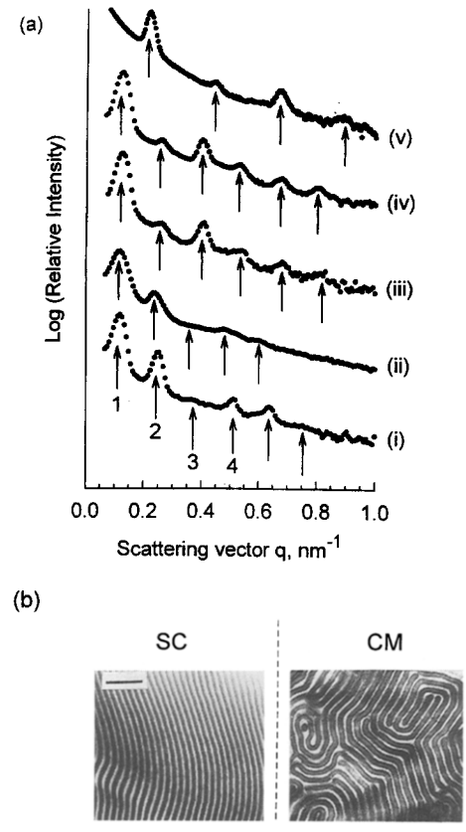

Figure 3 Microphase texture of alternating PS and PEP lamellae. (a) Room-temperature SAXS curve for (i) SEP35 (SC), (ii) SEP35 (CM), (iii) SEP50 (SC), (iv) SEP50 (CM), (v) SEPS50 (SC). (b) Representative TEM micrographs showing one view for SC and CM samples of SEP50. The orthogonal view was similar to the one shown for each sample. The scale bar of 200 nm applies to both micrographs

with a diamond knife. Samples were cut parallel and normal to the surface of the polymer film in order to obtain orthogonal planes, which is necessary to distinguish between the various microphase textures. For other sample preparations, ultrathin sections were obtained by cryomicrotomy at temperatures below − 70°C using an MT2B ultramicrotome equipped with a CR21 cryoattachment (RMC, Inc.) and a glass knife. The cryosections were isolated on Formvar and carbon coated microscope grids and stained at room temperature by exposure to the vapours from 0.5% aqueous RuO_4 solution for 5 min. No difference was observed in the results obtained from the two sectioning methods.

RESULTS AND DISCUSSION

Microphase structure

Long-range order. Most of the block copolymers exhibited long-range order in their microphase texture (see *Figures 1–3*). The microstructure of the SEP10 diblock copolymer consisted of PS spheres arranged on a cubic lattice (*Figure 1*). The SAXS data are plotted as the logarithm of the relative scattered intensity, $\log I(q)$, *versus* scattering vector, q, where $q = 4\pi(\sin\theta)/\lambda$, θ is one-half the scattering angle and λ is the X-ray wavelength. $I(q)$ is the product of the structure factor $S(q)$, which characterizes the spatial arrangement of the scattering entities, and the particle form factor $P(q)$ which characterizes their geometrical shape. The vertical arrows in *Figure 1*a indicate the positions of the scattering maxima, and the presence of higher-order maxima indicates substantial order of the microstructure. The scattering vector at the position of the first-order maximum, q^*, was used to estimate the characteristic dimension or period, D, of the microstructure using Bragg's Law, $D = 2\pi/q^*$. The values of D for SEP10 and the other block copolymers are given in *Table 2*.

The ratios of the scattering vectors at the maxima, q_m/q^*, where $m = 1, 2, 3,...$ is the order of the maximum and $q_1 = q^*$, were used to determine the specific microphase texture associated with each SAXS curve. The values of q_m/q^* for SEP10 in *Figure 1*a were about $1:\sqrt{2}:\sqrt{3}:\sqrt{4}$, which corresponds to cubic packing of spheres. Some details of the particle form factor for spheres are also seen in *Figure 1*a and are marked by diagonal arrows. Similar results were obtained for solution-cast and compression-moulded specimens, though the structure factor of the solution-cast sample

Table 2 Microphase textures and microstructure parameters

Polymer	Texture [a,b]	D (nm) [c]	R (nm) [d]	f_{PS} [e]	ϕ_{PS} [f]
SEP10	BCC spheres	25.0	7.8	0.090	0.089
SEP20	HCP cylinders	40.4	10.0	0.167	0.171
SEP35	Lamellae	53.1	8.2	0.310	0.309
SEP50	Lamellae	49.9	11.3	0.455	0.452
SEPS9	LLP spheres +	21.3	3.7 [g]	–	0.074
	HCP cylinders	≈ 30 [a]	≈ 10 [a]	–	
SEPS21	HCP cylinders	23.6	6.0	0.176	0.182
SEPS50	Lamellae	29.0	6.6	0.456	0.456
27SEP10	LLP spheres	22.6	6.3 [g]	–	0.080
27SEP18	LLP spheres [h]	23.3	≈ 7.5 [a]	–	0.155
27SEP50	Lamellae	25.6	5.9	0.462	0.446

[a] Determined by TEM.
[b] Determined by SAXS. The texture refers to the spatial arrangement of the PS domains—BCC for body-centered-cubic, HCP for hexagonal-close-packed, LLP for liquid-like packing.
[c] Characteristic morphological dimension $D = 2\pi/q^* = d_{hkl}$, $(hkl) = (110)$ for BCC, (100) for HCP.
[d] Radius of PS sphere, PS cylinder, or average half-thickness of PS lamella.
[e] Volume fraction of PS phase calculated from SAXS data.
[f] Volume fraction of PS phase calculated from w_{PS}.
[g] Calculated from Guinier analysis.
[h] TEM indicated regions where ill-defined PS cylinders were also present.

was better resolved, *cf.* curves (i) and (ii) in *Figure 1*a. The solid line in *Figure 1*a for the solution-cast sample corresponds to $P(q)$ for a hard non-elliptic sphere[30] with a radius, R, of 7.8 nm.

The packing symmetry of the PS spheres was determined by space-filling calculations assuming perfect packing order and sharp interphase boundaries using the following formulas:

$$\text{Simple} - \text{cubic (SC)}: \; f_{PS} = (4/3)\pi(R/D)^3 \quad (1)$$

$$\text{Face} - \text{centred} - \text{cubic (FCC)}: \; f_{PS} = (16/27)\pi\sqrt{3}(R/D)^3 \quad (2)$$

$$\text{Body} - \text{centred} - \text{cubic (BCC)}: \; f_{PS} = (\sqrt{8}/3)\pi(R/D)^3 \quad (3)$$

where f_{PS} = volume fraction of the PS phase, $D = d_{hkl} = 2\pi/q^*$, and (hkl) = (100) for SC, (111) for FCC and (110) for BCC. The experimentally determined values of D = 25.0 nm and R = 7.8 nm give f_{PS} = 0.127, 0.098 and 0.090 for SC, FCC and BCC packing, respectively. BCC packing best corresponds to the PS volume fraction measured by ^{1}H-NMR analysis, ϕ_{PS} = 0.089, and that assignment is confirmed by the TEM micrographs in *Figure 1*b.

When the PS content of a diblock or triblock copolymer was *ca.* 20 wt.%, samples SEP20 and SEPS21, the microstructure consisted of PS cylinders dispersed in a PEP continuous matrix (see *Figure 2*). The maxima in $S(q)$ for the SAXS curves in *Figure 2*a correspond to ratios $q_m/q^* \approx 1:\sqrt{3}:2:\sqrt{7}$: ..., which conforms to hexagonal-close-packed (HCP) cylinders, which is consistent with the TEM micrographs in *Figure 2*b. As with the SEP10 materials, the solution-cast and compression-moulded specimens had similar textures, but the microstructure was better developed in the solution-cast specimens. The radius, R, of the PS cylinders, determined by fitting the $P(q)$ for a hard right-circular cylinder of infinite length[31] (the solid curves in *Figure 2*a) with the minima in the experimental SAXS curve (the slanted arrows), was 10.0 nm and 6.0 nm for SEP20 and SEPS21, respectively (see *Table 2*). For perfect packing order and sharp interphase boundaries, the volume fraction of HCP cylinders is given by:

$$f_{PS} = (\sqrt{3}/2)\pi(R/D)^2 \quad (4)$$

where $D = d_{100} = 2\pi/q^*$. The value of f_{PS} calculated from equation (4) for SEP20 and SEPS21 was in good agreement with the volume fraction, ϕ_{PS}, determined from ^{1}H-NMR analysis (see *Table 2*).

When the PS content of the block copolymers was 35–50% (wt), an alternating lamellar microstructure was observed (*Figure 3*). The maxima in $S(q)$ for the SAXS curves in *Figure 3*a correspond to $q_m/q^* \approx 1, 2, 3, 4, 5, ...$, which is typical of a lamellar texture, and this is confirmed by the TEM micrographs shown in *Figure 3*b. The SAXS data in *Figure 3*a exhibit selective suppression, sometimes bordering on extinction, of the intensity of specific scattering maxima due to the particle shape factor of the lamellar stacks[30]. The suppression occurs for the maximum in $S(q)$ of order $\approx i/\phi_{PS}$, where i = 1, 2, 3, ..., *e.g.* the second- and fourth-order maxima were suppressed for SEP50, SEPS50 and 27SEP50, while the third- and sixth-order maxima were suppressed for SEP35. The volume fraction of the PS phase calculated using Vonk's method for lamellar stacks[30] agreed well with the volume fractions determined by ^{1}H-NMR (see *Table 2*).

Liquid-like short-range order. Two of the lower-molecular-weight diblock copolymers, 27SEP10 and 27SEP18, did not exhibit long-range microstructural order. Their SAXS curves (*Figure 4*a), showed only a single broad maximum in $S(q)$ in addition to $P(q)$ for spheres, which indicates a microstructure of PS spheres with liquid-like packing (LLP). The TEM micrographs in *Figure 4*b support that assignment, though the 27SEP18 sample (not shown) also had regions where the PS spheres coalesced into short poorly-developed cylinders. That latter observation is not surprising, because the composition of 27SEP18 is expected to be near the phase boundary between the spherical and cylindrical textures. Concentration fluctuations during the TEM sample preparation may have been responsible for the two different textures seen in 27SEP18. A similar LLP texture was recently reported for a polystyrene–*block*-polyisoprene–*block*-polystyrene copolymer by Sakamoto *et al.*[32], which they attributed to a lattice disordering transition that occurred between a BCC microphase and the disordered phase.

The average radius of the PS spheres estimated from the TEM micrographs was 6.5 nm and 7.5 nm for 27SEP10 and 27SEP18, respectively. However, the best fit of $P(q)$ for hard spheres to the SAXS curves (the solid curves in *Figure 4*a) was obtained for R = 11.8 nm for both polymers. The difference in the value of R determined by the two methods may be due to a distribution of sphere sizes, as is suggested by the non-linearity of the Guinier plot[30,31] for 27SEP10, curve (i) in *Figure 5*. $I(q)$ for a bimodal distribution of sphere sizes is[30,31]

$$I(q) = C[w_1 R_{g,1}^3 \exp(-q^2 R_{g,1}^2/3) + w^2 R_{g,2}^3 \exp(-q^2 R_{g,2}^2/3)] \quad (5)$$

where C is a constant and w_i and $R_{g,i}$ are the weight fraction and radius of gyration of the ith species, respectively. A combination of 96% spheres with R_g = 4.9 nm and 4% spheres with R_g = 28.5 nm accounts for the scattering

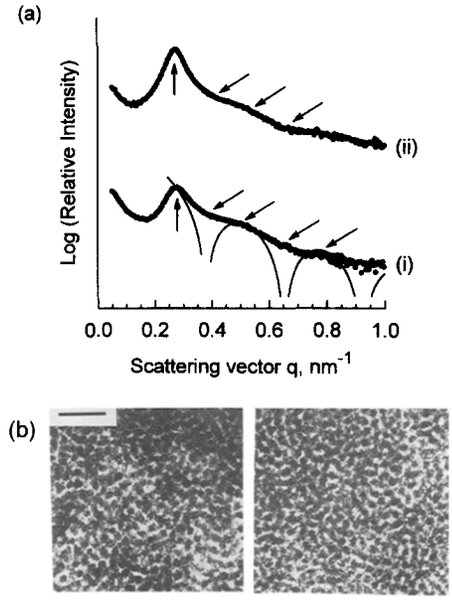

Figure 4 Microphase texture of LLP spheres of PS. (a) Room-temperature SAXS curve for (i) 27SEP10 and (ii) 27SEP18. The solid line represents the theoretical $P(q)$ function for a hard sphere of radius R = 11.8 nm. (b) TEM micrographs showing orthogonal views of the texture of LLP spheres for 27SEP10. The scale bar of 100 nm applies to both micrographs

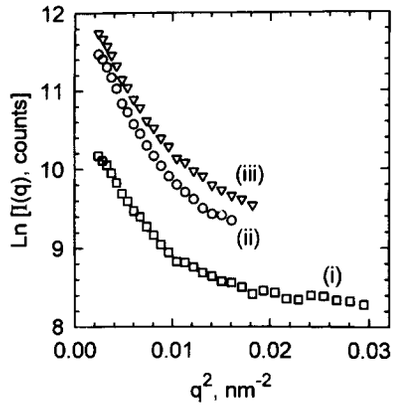

Figure 5 Guinier plot for (i) 27SEP10 (□), (ii) SEPS9 (SC) (○), (iii) SEPS9 (CM) (▽)

data in the Guinier region for 27SEP10. $R_g = 4.9$ nm corresponds to $R = 6.3$ nm, which agrees well with the $R = 6.5$ nm PS-sphere size estimated from the micrographs in *Figure 4*b. Using an analysis with more than two sphere sizes does not appreciably change the result that the majority of the spheres have radii of the order of 6 nm, but a small amount of domains with much larger radii are also present. In fact, the larger domains may be due to coalescence of the smaller domains and may also account for the poorly-developed cylinders observed in the micrographs for 27SEP18.

Triblock copolymer SEPS9. The SAXS and TEM of a solution-cast specimen of SEPS9 were particularly distinctive. The SAXS data, curve (i) in *Figure 6*a, showed three maxima in $S(q)$ with $q_m/q^* = 1{:}1.28{:}2$, which corresponds to neither BCC nor HCP textures, and a form factor for spheres. The TEM micrograph for this sample (*Figure 6*b) shows two very different textures—LLP spheres of PS with $R \approx 4$ nm and HCP cylinders of PS with $R \approx 10$ nm and $d_{100} \approx 30$ nm. The PS cylinders appear to break into spheres at the boundary between the two regions. The SAXS curve (i) in *Figure 6*a represents a combination of the scattering from the two different textures, and their dimensions are summarized in *Table 2*. The third maximum was used to calculate the characteristic dimension, D, of the spherical microdomains, since that peak corresponded most closely to the single maximum in the structure factor for 27SEP10. Generally, for constant composition, the texture of a triblock copolymer is expected to be similar to that of a diblock copolymer of half the molecular weight.

The SAXS data for curve (i) in *Figure 6*a could be fit equally well with a form factor for spheres with radius $R = 11.5$ nm or for cylinders with $R = 10.3$ nm, as shown by the solid and dotted lines, respectively, in *Figure 6*a. That cylinder radius is consistent with the cylinders observed in the TEM ($R \approx 10$ nm), but the average radius of the spheres observed in the TEM was much smaller than 11.5 nm. For HCP cylinders, a first-order scattering maximum should occur at $q^* = 2\pi/d_{100}$. From the TEM, $d_{100} = 30$ nm, so that $q^* = 0.21\ \text{nm}^{-1}$, which is consistent with the SAXS peak at $q = 0.19\ \text{nm}^{-1}$ in *Figure 6*a. However, the first-order maximum at $q = 0.15\ \text{nm}^{-1}$ ($d \approx 42$ nm) does not appear to correspond to any feature observed in the TEM micrograph and its origin is unclear. The SAXS curve (i) in *Figure 6*a for solution-cast samples of SEPS9 was reproducible over different regions of several films, so it is unlikely that this is an artifact.

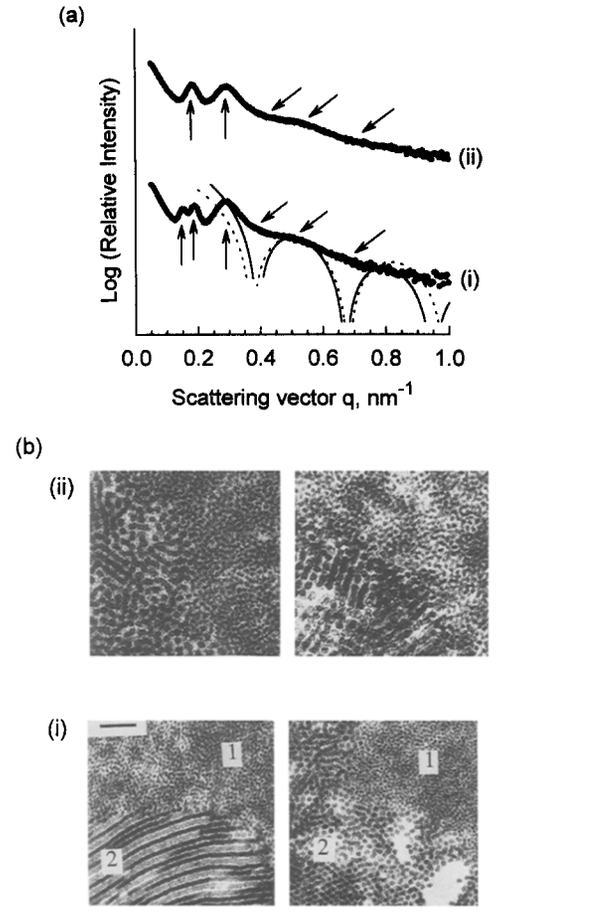

Figure 6 Microphase texture of SEPS9 triblock copolymer. (a) Room-temperature SAXS curve for (i) SEPS9 (SC) and (ii) SEPS9 (CM). The solid and dotted lines represent the theoretical $P(q)$ function for a hard sphere of $R = 11.5$ nm and an infinitely long cylinder of $R = 10.3$ nm, respectively. (b) TEM micrographs showing orthogonal views of the microphase texture for SEPS9 samples described in (i) and (ii) in part (a). Regions 1 and 2 correspond to a texture of LLP spheres and HCP cylinders of PS, respectively. The scale bar denotes a dimension of 200 nm and applies to all four micrographs

The SAXS curve for the compression-moulded SEPS9, shown as curve (ii) in *Figure 6*a, also indicates a complicated microstructure. Two maxima in the structure factor and a form factor similar to that for the solution-cast sample were observed. The relative positions of the two peaks, $q_m/q^* = 1{:}1.64$, does not correspond to any of the usual block copolymer microstructures. The peak positions are, however, consistent with the two textures seen in the micrographs in *Figure 6*b, curve (ii): (1) LLP spheres of PS with $R \approx 4$ nm, and (2) poorly-formed PS cylinders with $R \approx 11$ nm.

Guinier analysis of the SAXS profiles for the solution-cast and compression-moulded SEPS9 scattering curves indicated that 98 wt.% of the PS domains existed as LLP spheres having $R_g = 2.9$ nm, which corresponds to a $R = 3.7$ nm. That radius agrees well with the TEM results of $R \approx 4$ nm.

The data for SEPS9 indicate that an equilibrium microstructure was not obtained in either the solution-cast or compression-moulded samples. A microstructure of spherical PS domains was expected for that composition. Because SEPS9 also had the lowest viscosity of any of the triblock copolymers studied, it is surprising that only for this sample was equilibrium not achieved. It may be that because of the low viscosity, flow of the material during

sample preparation may have induced a microphase transition from spheres to cylinders. For example, Jackson *et al.*[33] recently reported the coexistence of two non-equilibrium cylindrical microstructures of different symmetries in a poly(styrene–*b*-butadiene–*b*-styrene) copolymer that was sheared near T_{ODT}. For the SEPS9, T_{ODT} = 80°C, which was close to the annealing temperature of 70°C that was used for the sample preparation.

Effects of sample preparation. The development of long-range order of the microstructure was considerably less for the compression-moulded block copolymer samples than for the corresponding solution-cast samples as long as T_{ODT} was greater than the moulding temperature of 200°C. For example, SAXS and TEM results for compression-moulded SEP20 (T_{ODT} = 325°C) revealed poorly-ordered cylindrical PS domains in contrast with the well-ordered HCP arrangement observed for solution-cast SEP20 (see *Figure 2*). Similarly, the lamellar microstructure of SEP35 was much more longer-range when the material was solution-cast *versus* compression-moulded. Those results are not surprising, because of the high melt viscosities involved in compression-moulding and the relatively short time (~2 h) during which the melt solidifies. Such conditions restrict molecular mobility, which is necessary to achieve a well-ordered microphase texture. In contrast, the relatively higher molecular mobility of the polymer in solution and slow drying times are more conducive to the attainment of well-ordered microstructures closer to equilibrium.

When the T_{ODT} of the block copolymer was below the moulding temperature of 200°C, a well-ordered microstructure comparable to that achieved by solution casting was obtained for compression-moulded specimens. That is illustrated by the SAXS and TEM results for SEP10 (T_{ODT} = 185°C) in *Figure 1* and SEPS21 (T_{ODT} = 157°C) in *Figure 2*.

Thermotropic microphase transitions

In the discussion that follows, unless otherwise stated, all DMTA and temperature-resolved SAXS results refer to solution-cast samples.

Order–disorder transitions. G'' and tan δ data at a frequency of 0.1 Hz for the block copolymers are shown in *Figures 7 and 8*, respectively. Because the ODT is expected to be a first-order transition[1], T_{ODT} was defined from the dynamic shear moduli data as the discontinuity in the slope of G' *versus* temperature; e.g. T_{ODT} = 185°C for SEP10 (*Figure 7*a). Tan δ may be a more sensitive indicator of the onset of the ODT. Near the ODT, viscous contributions to the viscoelastic behaviour become dominant as the material begins to undergo bulk flow as a result of enhanced microphase mixing. This is manifested by a steep increase in tan δ, and T_{ODT} may be defined by the discontinuity in the temperature dependence of tan δ. The tan δ data in *Figure 8*a also indicate a T_{ODT} = 185°C for SEP10. The vertical and diagonal arrows in *Figures 7 and 8* denote T_{ODT} and T_g of the PS phase, respectively. The T_{ODT} values calculated from the DMTA data for the different block copolymers shown in *Figures 7 and 8* are given in *Table 3*.

Figure 9 shows the temperature-resolved SAXS profiles for SEPS21 measured while heating from 40°C to 280°C and then cooling back to 40°C. The scattering curve did not change upon heating between 40 and 170°C, but above 170°C, the higher-order maxima in the structure factor disappeared and the intensity of the first-order maximum decreased markedly, which is characteristic of the ODT. A single broad maximum in the structure factor persists above T_{ODT} (175°C) due to correlation between the different blocks in the disordered state and the incompressibility of the copolymer melt. The changes in the SAXS curve were recovered upon cooling the SEPS21 from 280 to 40°C, which demonstrates the reversibility of the ODT. Different

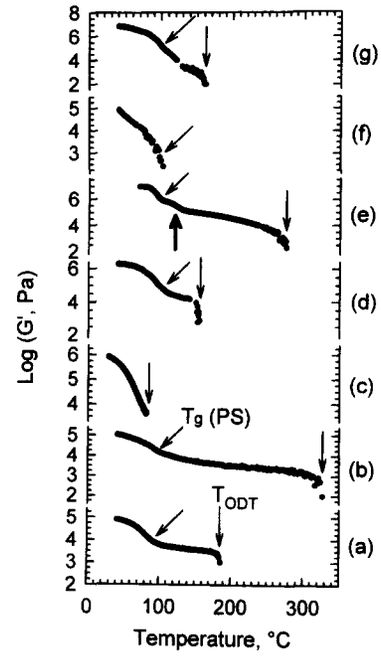

Figure 7 DMTA measurements showing the temperature dependence of the dynamic shear storage modulus, G', at 0.1 Hz for solution-cast block copolymers. Vertical and diagonal arrows indicate the order–disorder transition (ODT) and the glass transition of the PS microphase, respectively. (a) SEP10, (b) SEP20, (c) SEPS9, (d) SEPS21, (e) SEPS50, (f) 27SEP18, (g) 27SEP50. The bold arrow on curve (e) indicates an order–order transition (OOT) in SEPS50 between conventional lamellar (LAM) and perforated lamellar (PL) microphase textures

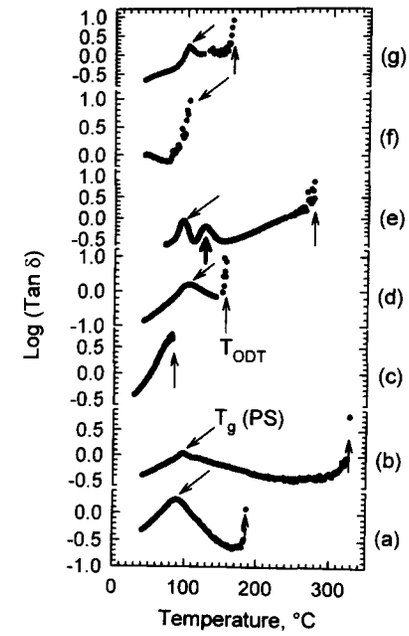

Figure 8 DMTA measurements showing the temperature dependence of the dynamic loss tangent, tan δ, at 0.1 Hz for solution-cast block copolymers. (a) SEP10, (b) SEP20, (c) SEPS9, (d) SEPS21, (e) SEPS50, (f) 27SEP18, (g) 27SEP50. Arrows have the same meaning as in Figure 7

Table 3 Microphase transition temperatures and related parameters

Polymer	T_{ODT} (°C) (DMTA)	T_{ODT} (°C) (SAXS)	$T_{ODT,MF}$ (°C) (SAXS)	$T_{S,MF}$ (°C) (SAXS)	T_{OOT} (°C)	Exponent p in $D \sim T^p$
SEP10	185	185	220	175	n/a	0
SEP20	325	– [a]	– [a]	– [a]	n/a	n/a
SEP35	– [a]	– [a]	– [a]	– [a]	n/a	n/a
SEP50	– [a]	– [a]	– [a]	– [a]	n/a	n/a
SEPS9	80 [d]	80 [d], 230 [e] (70 [d], 220 [e]) [c]	n/a	n/a	n/a	n/a
SEPS21	157	175 (145) [c]	260 (210) [c]	212 (175) [c]	n/a	−0.029 (−0.022) [c]
SEPS50	275	– [a]	– [a]	– [a]	125 [f]	−0.021
27SEP10	– [b]	80	80	49	n/a	n/a
27SEP18	– [b]	190	190	165	n/a	−0.021
27SEP50	– [b]	– [a]	– [a]	– [a]	162 [g]	−0.021

[a] Beyond experimentally accessible temperatures.
[b] Not observed due to very low modulus value.
[c] Data from cooling scan.
[d] LLP phase of PS spheres.
[e] HCP phase of PS cylinders.
[f] OOT between lamellar and perforated lamellar textures.
[g] OOT between lamellar texture and a high-temperature texture of unknown geometry.

temperatures were obtained, however, for the transition between the ordered and disordered microstructure upon heating (T_{ODT} = 175°C) and cooling (T_{MST} = 145°C), and the maxima in the structure factor obtained upon cooling the sample from the disordered melt were not as sharp as for the original sample. The thermodynamic ODT and MST should be identical, and the hysteresis between the ODT and MST is most likely due to kinetic effects resulting from the high viscosity of the melt. Similarly, the more poorly developed order of the microstructure in the cooled melt as evident from the broader, more diffuse maxima in the structure factor, is also consistent with the increased difficulty in developing a well-ordered microstructure from a viscous melt compared with a solution.

The ODT was defined by a discontinuity in the slope of the temperature-dependence of the intensity of the first-order scattering maximum, $I(q^*)$[13,34] or by a discontinuity in a plot of the SAXS data as $1/I(q^*)$ *versus* $1/T$, where T is the absolute temperature in Kelvin[35–40], see the vertical downward arrows marked (iii) in *Figure 10*. Either analysis gave comparable values, e.g. T_{ODT} = 185°C for SEP10.

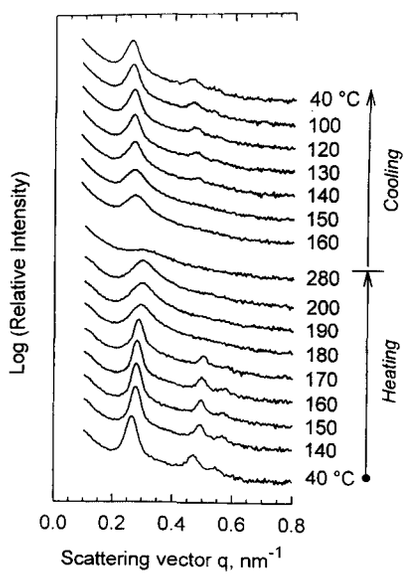

Figure 9 Temperature-resolved SAXS profiles for solution-cast SEPS21 obtained upon heating between 40 and 280°C followed by cooling to 40°C

T_{ODT} was obtained by both DMTA and SAXS measurements for two other materials, SEPS9 and SEPS21. For SEPS9, the DMTA result corresponded with the disappearance of the LLP microphase (see *Table 3*), which, as discussed above, was the dominant texture in that sample. However, for SEPS21, T_{ODT} obtained by DMTA was 18°C lower than the value determined from the SAXS heating experiments, see *Table 3*. By itself, that result is not surprising since the two techniques, DMTA and SAXS, probe different phenomena. Temperature-resolved SAXS provides a direct measurement of the size and periodicity of the microstructure, while the DMTA experiment probes the molecular motions of the chain segments. In this case, the DMTA detects the motions of the chain that precede disordering, even though the SAXS results indicate that some remnants of the structure may persist to higher temperature. Winey *et al.*[41] reported similar differences in

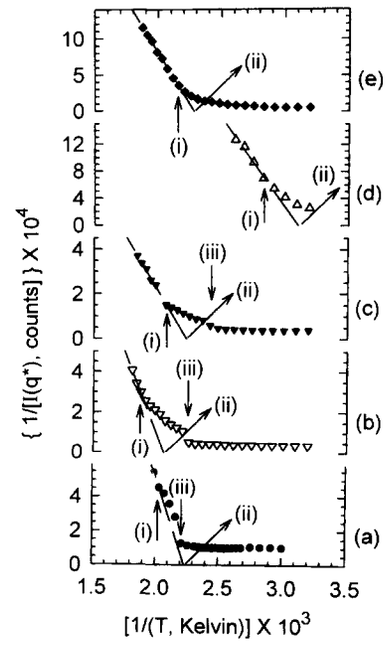

Figure 10 Plots of $1/I(q^*)$ *versus* $1/T$ for solution-cast block copolymers. Arrows (i), (ii) and (iii) on each plot indicate $1/T_{ODT,MF}$, $1/T_{S,MF}$, and $1/T_{ODT}$, respectively, *cf.* Table 3. (a) SEP10, (b) SEPS21, heating scan, (c) SEPS21, cooling scan, (d) 27SEP10, (e) 27SEP18

the T_{ODT} of PS–PI diblock copolymers measured by dynamic shear and SAXS experiments. The agreement of the transition for SEP10 and SEPS9 may be a consequence of the lower viscosity of those polymer melts.

There was a pronounced non-linearity in the $1/I(q^*)$ *versus* $1/T$ plots in *Figure 10* for the data when $T > T_{ODT}$, which was due to composition fluctuations that cause non-mean-field behaviour[34,35,40]. A linear region of the plot at higher temperatures was used to calculate the mean-field ODT temperature, $T_{ODT,MF}$, and the mean-field spinodal temperature, $T_{S,MF}$, following the approach of Sakamoto and Hashimoto[40], in which $T_{ODT,MF}$ is defined by the temperature at which the $1/I(q^*)$ *versus* $1/T$ relationship deviates from linearity and $T_{S,MF}$ is calculated from the extrapolation of the linear portion of the curve to $1/I(q^*) = 0$. $T_{ODT,MF}$ and $T_{S,MF}$ are denoted in *Figure 10* by the vertical upward arrows marked (i) and the diagonal arrows marked (ii), respectively, and all calculations are summarized in *Table 3*. In some cases, e.g. for SEP10, the number of points used to draw the straight line were limited, so the uncertainty in the $T_{ODT,MF}$ may be appreciable.

The characteristic dimension, D, of the microstructure calculated using Bragg's law and the scattering vector of the first maximum in the structure factor was only weakly dependent upon temperature (not shown). For SEP10, D was invariant with temperature for $T < T_{ODT}$, and no change occurred at T_{ODT} or for $T > T_{ODT}$. For the other block copolymers $D \sim T^{-p}$, where $p = 0.021$–0.029. This result is in stark contrast to the results of Hashimoto *et al.*[42] who reported that for PS–PI diblock copolymers, $D \sim T^{-1/3}$ for $T < T_{ODT}$ and $D \sim T^0$ for $T > T_{ODT}$, and of Sakurai *et al.*[43] who reported that $D \sim T^{-0.425}$ for an SEP diblock copolymer when $T < T_{ODT}$.

The ODT for SEP20 was not observed by temperature-resolved SAXS experiments, which were limited to 280°C. DMTA indicated that $T_{ODT} = 325$°C for that material. T_{ODT} is expected to increase as the volume fraction of the minority component increases[1,6,8–10]. Therefore, for SEP35 and SEP50 $T_{ODT} > 325$°C, and as a result no ODT was observed by either SAXS or DMTA for those block copolymers. Although the limited GPC analyses performed indicated little degradation when the polymers were heated above 200°C, one might expect some degradation to occur, especially when the samples were heated above 300°C. Degradation would be expected to lower the observed T_{ODT}, so the high values for T_{ODT} reported above should probably be considered lower limits.

Order–order and order–disorder transitions. DMTA measurements for SEPS50 revealed a post-T_g relaxation occurring centered at *ca.* 125°C, as marked by the bold arrow in curves (e) in *Figures 7 and 8*. Dynamic-shear heating and cooling experiments demonstrated that mechanical relaxation was reversible, and TEM micrographs obtained on samples annealed above and below the transition (*Figure 11*) indicated that it was a thermally-reversible order–order transition (OOT) between conventional lamellar (LAM) and perforated lamellar (PL) microphases. (Note that the microstructure shown in *Figure 11*b is not of cylindrical microdomains. The PL texture was confirmed by extensive TEM and SAXS analyses[44].) The LAM phase comprises alternating PS and PEP lamellae, and the PL phase consists of alternating PS and PEP lamellae where the PS lamellae are bridged by hexagonal-packed connectors that perforate the PEP lamellae.

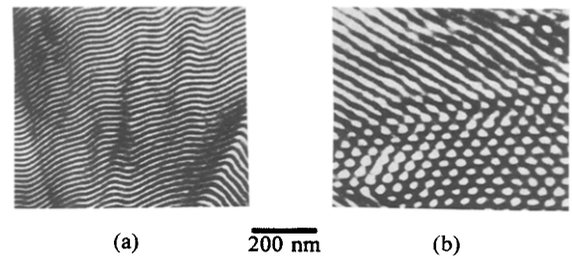

Figure 11 TEM micrographs indicating an order–order transition in solution-cast SEPS50. (a) For a sample annealed at 100°C and cooled slowly to room temperature prior to staining, showing a conventional lamellar microphase texture. (b) A different sample that was annealed at 200°C and then quenched in liquid nitrogen prior to staining, showing a perforated lamellar texture. The scale bar of 200 nm applies to both micrographs

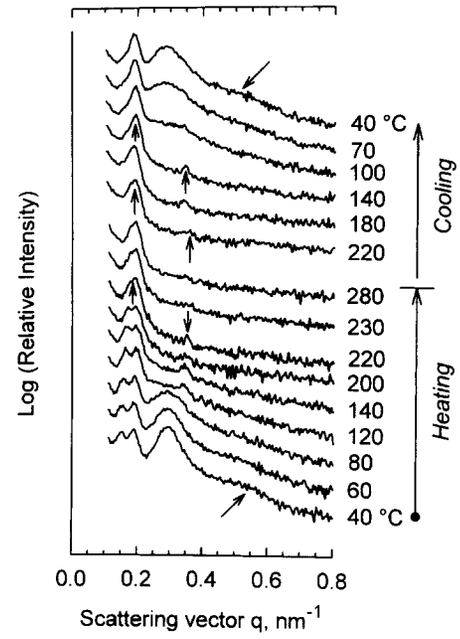

Figure 12 Temperature-resolved SAXS profiles for solution-cast SEPS9 obtained upon heating between 40 and 280°C followed by cooling to 40°C. Diagonal and vertical arrows indicate the maximum of the particle form factor and structure factor, respectively

SEPS9 triblock copolymer. As discussed earlier in this paper, the solution-cast SEPS9 sample exhibited two different microphase textures—LLP spheres of PS and HCP cylinders of PS. A sharp T_{ODT} of SEPS9 was not observed by DMTA experiments (see *Figure 7*) because of the relatively low viscosity of that sample above 80°C. *Figure 12* shows the temperature-resolved SAXS curves during heating and cooling a solution-cast SEPS9 sample between 40–280°C. The particle form-factor for spheres, indicated by the diagonal arrow on the bottom curve, gradually diminished with increasing temperature between 40–80°C and vanished at 80°C due to the ODT of the LLP microphase of PS spheres. The intensity of the third-order maximum at $q = 0.29$ nm^{-1} decreased between 80–120°C, eventually revealing a maximum in the structure factor at $q = 0.34$ nm^{-1} that may have been present, but concealed by the peak at $q = 0.29$ nm^{-1}, at lower temperatures. When the temperature was increased from 120°C to 220°C, the maximum in the structure factor at $q = 0.15$ nm^{-1} disappeared. At 220°C, the structure factor exhibited maxima at $q = 0.19$ nm^{-1} and 0.34 nm^{-1}, which gives a ratio q_m/q^*

= 1:1.79. That ratio is close to the value expected for a HCP microstructure ($q_m/q^* = 1:\sqrt{3}$). The maximum in the structure factor at $q = 0.34\ nm^{-1}$ vanished at 230°C, which corresponds to the T_{ODT} of the HCP microphase. The SAXS peak at $q = 0.19\ nm^{-1}$ that persisted between 230–280°C arises from a correlation hole in the disordered melt that arises from the structure of the block copolymer.

The scattering signature of the HCP microphase, i.e. peaks in the structure factor at $q = 0.19\ nm^{-1}$ and $0.34\ nm^{-1}$, was recovered at $T_{MST} = 220$°C upon cooling the disordered melt (*Figure 12*). That result was surprising in that, based on the composition of the block copolymer, one would expect the equilibrium microstructure to be spherical PS microdomains. A LLP microphase of PS spheres was recovered as the temperature was further lowered ($T_{MST} = 70$°C), as evidenced by the development of the maximum in the structure factor at $q = 0.29\ nm^{-1}$ and the particle form-factor for spheres (denoted by the diagonal arrow in the top profile in *Figure 12*). The high intensity of the maximum at $q = 0.29\ nm^{-1}$ concealed the second-order maximum of the HCP microphase at $q = 0.34\ nm^{-1}$ for $T < 100$°C. Two first-order maxima in the structure factor are evident in the final SAXS profile at 40°C—one at $q = 0.19\ nm^{-1}$ corresponding to the HCP texture of PS cylinders, and the other at $q = 0.29\ nm^{-1}$ due to the LLP microphase of PS spheres.

The maximum at $q = 0.15\ nm^{-1}$ that was observed for the as-cast sample did not reappear after heating and cooling from 280°C, *cf.* the top and bottom SAXS curves in *Figure 12*. The top SAXS curve, which was obtained after completing the heating–cooling cycle, was similar to the room-temperature SAXS curve for the compression-moulded SEPS9 shown in *Figure 6*. That result further supports the conclusion stated earlier in this paper that a non-equilibrium microstructure was obtained in the solution-cast SEPS9 sample. Although the reason for this was not determined, it may have resulted from flow of the solvent-plasticized sample, which had a relatively low viscosity compared with the other block copolymer samples. Shear flow has been shown to promote non-equilibrium microstructures in other block copolymers[33,45].

The microstructure and its temperature dependence for the compression-moulded SEPS9 were less complicated than for the solution-cast sample (*Figure 13*). The intensity of the particle form-factor, indicated by the arrow, and the second-order maximum in the structure factor at $q = 0.29\ nm^{-1}$ decreased gradually between 40 and 100°C, which corresponded to the disordering of the LLP microphase of PS spheres ($T_{ODT} \approx 80$°C). The intensity of the first-order maximum at $q = 0.18\ nm^{-1}$ decreased gradually with increasing temperature between 40 and 280°C. Unexpectedly, the 280°C SAXS curves for the compression-moulded and solution-cast samples (*cf. Figures 12 and 13*) were significantly different even though both were presumably disordered, homogenous melts of the block copolymer. The correlation hole peak at $q = 0.19\ nm^{-1}$ that was still prominent at 280°C for the solution-cast sample (*Figure 12*) is barely perceivable for the compression-moulded sample (*Figure 13*). Although the reason for this disparity is not clear, the data for the solution-cast sample, which possessed a HCP microphase before it disordered, suggest that some remnant of the HCP microstructure may have remained at 280°C in the experiment shown in *Figure 12*. That may also explain why the HCP microstructure reappeared upon cooling the solution-cast sample from 280°C. That hypothesis suggests a memory of the

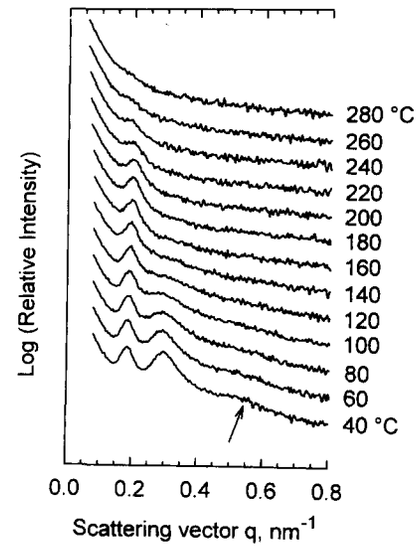

Figure 13 Temperature-resolved SAXS profiles for compression-moulded SEPS9 obtained upon heating. The diagonal arrow indicates the maximum of the particle form factor

mesophase texture above T_{ODT} similar to what has been previously observed with semi-crystalline polymers above the melting point and liquid crystalline polymers above the clearing temperature. Based on the limited data shown here, that conclusion must be considered speculative, though experiments in which the block copolymer is annealed in the isotropic phase for varying times should delineate its validity—that is, any memory of the microphase above T_{ODT} is expected to be time-dependent.

CONCLUSIONS

Diblock and triblock copolymers of polystyrene (PS) and poly(ethylene-*alt*-propylene) (PEP) were synthesized and their microstructure textures identified by SAXS and TEM. As the composition was varied from 10 wt.% to 50 wt.% PS, the microstructure changed from spherical domains of PS to cylindrical domains of PS to alternating PS and PEP lamellae. The packing arrangement of the PS domains depended on the molecular weight, block architecture and method of sample preparation. At the lowest PS composition of *ca.* 10 wt.%, doubling the molecular weight from *ca.* $27\ kg\ mol^{-1}$ to *ca.* $50\ kg\ mol^{-1}$ at constant diblock architecture or changing the architecture from triblock to diblock at a constant molecular weight of *ca.* $50\ kg\ mol^{-1}$ caused the morphology to change from an amorphous liquid-like-packing (LLP) arrangement to a well-defined ordered body-centred-cubic (BCC) arrangement of PS spheres. At an intermediate composition of *ca.* 20 wt.% PS, a morphology of hexagonal-close-packed (HCP) cylinders of PS was present at the high molecular weight for both diblock and triblock architectures, while LLP spheres of PS with a minority of short, poorly-formed PS cylinders with no positional order were present at the lower molecular weight.

The development of morphological order in a compression-moulded block copolymer sample *vis-à-vis* the corresponding solution-cast sample was determined to a large extent by the relative values of the order–disorder transition temperature, T_{ODT}, and the moulding temperature, T_m. In general, for $T_{ODT} < T_m$, the microstructure order obtained by compression-moulding and solution-casting

were comparable, but when $T_{ODT} > T_m$, the order developed in the solution-cast samples was much better. The SEP50 diblock copolymer was an exception to that general rule.

For comparable composition and molecular weight, the T_{ODT} of the diblock copolymers was higher than for the corresponding triblock copolymers. The SEPS50 triblock copolymer exhibited a reversible order–order transition (OOT) between lamellar and perforated lamellar microphases prior to disordering. The 27SEP50 low-molecular-weight diblock copolymer also showed evidence of complex microphase behaviour, though it was not possible to uniquely determine the geometry of the high-temperature microstructure. The characteristic morphological dimension, D, of the block copolymers scaled with temperature, T, as $D \sim T^p$, where $-0.029 \leq p \leq -0.021$, for $T_g < T_{ODT}$ and as $D \sim T^0$ for $T > T_{ODT}$.

ACKNOWLEDGEMENTS

RAW and SM are grateful to the Office of Naval Research (Grant N00014-91-J-1564) and the International Programs Division of the National Science Foundation (Grant INT-9216859) for support of this research. CEW acknowledges support from CNRS. We also thank Dr. Dorab E. Bhagwagar, Dr. Pierre Lesieur and Prof. J. R. Knox for their assistance in collecting and interpreting the SAXS data, and Ms. Bridget Bartos for the GPC analyses.

REFERENCES

1. Bates, F. S. and Fredrickson, G. H., *Ann. Rev. Phys. Chem.*, 1990, **41**, 525.
2. Helfand, E. and Wasserman, Z. R., *Macromolecules*, 1976, **9**, 879.
3. Helfand, E. and Wasserman, Z. R., *Polym. Eng. Sci.*, 1977, **17**, 582.
4. Helfand, E. and Wasserman, Z. R., *Macromolecules*, 1978, **11**, 960.
5. Helfand, E. and Wasserman, Z. R., *Macromolecules*, 1980, **13**, 994.
6. Leibler, L., *Macromolecules*, 1980, **13**, 1602.
7. Ohta, T. and Kawasaki, K., *Macromolecules*, 1986, **19**, 2621.
8. Fredrickson, G. H. and Helfand, E., *J. Chem. Phys.*, 1987, **87**, 697.
9. Mayes, A. M. and Olvera de la Cruz, M., *J. Chem. Phys.*, 1989, **91**, 7228.
10. Lescanec, R. L. and Muthukumar, M., *Macromolecules*, 1993, **26**, 3908.
11. Thomas, E. L., Anderson, D. M., Henkee, C. S. and Hoffman, D., *Nature*, 1988, **334**, 598.
12. Hashimoto, T., Koizumi, S., Hasegawa, H., Izumitani, T. and Hyde, S. T., *Macromolecules*, 1992, **25**, 1433.
13. Almdal, K., Koppi, K. A., Bates, F. S. and Mortensen, K., *Macromolecules*, 1992, **25**, 1743.
14. Hamley, I. W., Koppi, K. A., Rosedale, J. H., Bates, F. S., Almdal, K. and Mortensen, K., *Macromolecules*, 1993, **26**, 5959.
15. Bates, F. S., Schulz, M. F., Khandpur, A. K., Förster, S., Rosedale, J. H., Almdal, K. and Mortensen, K., *Faraday Discuss.*, 1994, **98**, 1.
16. Förster, S., Khandpur, A. K., Zhao, J., Bates, F. S., Hamley, I. W., Ryan, A. J. and Bras, W., *Macromolecules*, 1994, **27**, 6922.
17. Khandpur, A. K., Förster, S., Bates, F. S., Hamley, I. W., Ryan, A. J., Bras, W., Almdal, K. and Mortensen, K., *Macromolecules*, 1995, **28**, 8796.
18. Sakurai, S., Kawada, H., Hashimoto, T. and Fetters, L. J., *Macromolecules*, 1993, **26**, 5796.
19. Hajduk, D. A., Gruner, S. M., Rangarajan, P., Register, R. A., Fetters, L. J., Honeker, C., Albalak, R. J. and Thomas, E. L., *Macromolecules*, 1994, **27**, 490.
20. Tung, L. H., Lo, G. Y. S. and Beyer, D. E., US Patent Nos. 4182818 and 4196153, 1980.
21. Tung, L. H., Lo, G. Y. S. and Beyer, D. E., *Macromolecules*, 1978, **11**, 616.
22. Tung, L. H. and Lo, G. Y. S., *Macromolecules*, 1994, **27**, 1680.
23. Tung, L. H. and Lo, G. Y. S., *Macromolecules*, 1994, **27**, 2219.
24. Bredeweg, C. J., Gatzke, A. L., Lo, G. Y. S. and Tung, L. H., *Macromolecules*, 1994, **27**, 2225.
25. Lo, G. Y. S., Otterbacher, E. W., Gatzke, A. L. and Tung, L. H., *Macromolecules*, 1994, **27**, 2233.
26. Eckert, R. J. A., US Patent No. 4156673, 1979.
27. McGrath, J. E., Wilkes, G. L., Ward, T. C., Broske, A. D., Lee, B., Yilgor, I., Bradley, D. J., Hoover, J. M. and Long, T. E., *New Elastomer Synthesis for High Performance Applications*. Noyes Data Corporation, Park Ridge, NJ, 1988.
28. Hahn, S. F., *J. Polym. Sci., Part A: Polym. Chem.*, 1992, **30**, 397.
29. Dubuisson, J. M., Dauvergne, J. M., Depautex, C., Vachette, P. and Williams, C. E., *Nucl. Instrum. Meth. Phys. Res.*, 1986, **A246**, 636.
30. Glatter, O. and Kratky, O., (eds), *Small Angle X-ray Scattering*. Academic Press, New York, 1982.
31. Guinier, A. and Fournet, G., *Small-angle Scattering of X-rays*. Wiley, New York, 1955.
32. Sakamoto, N., Hashimoto, T., Han, C. D., Kim, D. and Vaidya, N. Y., *Macromolecules*, 1997, **30**, 1621.
33. Jackson, C. L., Barnes, K. A., Morrison, F. A., Mays, J. W., Nakatani, A. I. and Han, C. C., *Macromolecules*, 1995, **28**, 713.
34. Almdal, K., Bates, F. S. and Mortensen, K., *J. Chem. Phys.*, 1992, **96**, 9122.
35. Bates, F. S., Rosedale, J. H. and Fredrickson, G. H., *J. Chem. Phys.*, 1990, **92**, 6255.
36. Hashimoto, T., Ijichi, Y. and Fetters, L. J., *J. Chem. Phys.*, 1988, **89**, 2463.
37. Hashimoto, T., Ijichi, Y. and Fetters, L. J., *Macromolecules*, 1989, **22**, 2817.
38. Owens, J. N., Gancarz, I. S., Koberstein, J. T. and Russell, T. P., *Macromolecules*, 1989, **22**, 3380.
39. Koberstein, J. T., Russell, T. P., Walsh, D. J. and Pottick, L., *Macromolecules*, 1990, **23**, 877.
40. Sakamoto, N. and Hashimoto, T., *Macromolecules*, 1995, **28**, 6825.
41. Winey, K. I., Gobran, D. A., Xu, Z., Fetters, L. J. and Thomas, E. L., *Macromolecules*, 1994, **27**, 2392.
42. Hashimoto, T., Shibayama, M. and Kawai, H., *Macromolecules*, 1983, **16**, 1093.
43. Sakurai, S., Hashimoto, T. and Fetters, L. J., *Macromolecules*, 1995, **28**, 7947.
44. Mani, S., Weiss, R. A., Hanh, S. F., Williams, C. E., Cantino, M. E. and Khairallah, L. H., unpublished work.
45. Koppi, K. A., Tirrell, M. and Bates, F. S., *J. Rheol.*, 1994, **38**, 999.
46. Hashimoto, T., Kawamura, T., Harada, M. and Tanaka, H., *Macromolecules*, 1994, **27**, 3063.